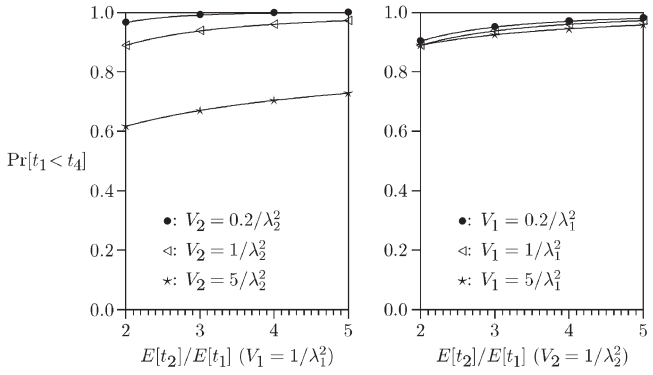

Fig. 2. Effects of λ_1/λ_2, V_1, and V_2 on $\Pr[t_1 < t_4]$.

the roaming group approach is much faster than that in the 3GPP approach. This figure also indicates that the variances of t_2 and t_3 have more impact on $\Pr[t_1 < t_4]$ than $E[t_2]/E[t_1]$ does. Therefore, to support this kind of routing services, reducing the variances of delays are essential.

Through the roaming software installed in the handsets, call setup is a transparent process where the call parties have the same call setup experience as before. The roaming gateway utilizes the short message protocol to download/update the mapping table in a handset. The table download operation is executed only when a new member is added to a roaming group. If the table size is too large to be included in one short message, the table is delivered via multiple short messages using the concatenated short message technique. The table update operation is executed only when the roamer moves to another country. In other words, the update frequency is typically very low, and our solution consumes little handset power (similar to the manipulation of address book in the handset). To enhance the security, the short message can be encrypted using the *Rivest–Shamir–Adleman* (RSA) or the identity-based schemes [7].

In the roaming group solution, existing telecom elements (e.g., HSS, MSC, and GMSC) and protocols (e.g., SS7 and short message protocol) are not modified. The telecom network is slightly modified by adding a plug-in roaming gateway (this plug-in's effort is very low). Therefore, the roaming group solution is an effective approach for reducing international call costs.

As a final remark, this solution is especially attractive for a group of travelers who roam to the same visited country and communicate with each other frequently during the trip.

REFERENCES

[1] Y.-B. Lin and A.-C. Pang, *Wireless and Mobile All-IP Networks*. New York: Wiley, 2005.

[2] J.-R. Lin, A.-C. Pang, and Y.-C. Wang, "iPTT: Peer-to-peer push-to-talk for VoIP," *J. Wireless Commun. Mobile Comput.*, vol. 8, no. 10, pp. 1331–1343, Dec. 2008.

[3] W.-E. Chen, "The deployment of IPv6 SIP-based VoIP applications," *Int. J. Internet Protocol Technol.*, vol. 1, no. 4, pp. 205–213, Aug. 2006.

[4] 3GPP. 3rd Generation Partnership Project, Tech. Spec. 3G TS 22.079, ver. 8.0.0 (2008-12), Tech. Spec. Group Services and System Aspects; Support of Optimal Routing, Service Definition—Stage 12008.

[5] Y.-B. Lin, "Reducing international roaming call costs with multiple mobile phone numbers," *IEEE Commun. Lett.*, vol. 12, no. 7, pp. 529–531, Jul. 2008.

[6] S.-R. Yang, "Dynamic power saving mechanism for 3G UMTS system," *Mobile Netw. Appl.*, vol. 12, no. 1, pp. 5–14, Nov. 2007.

[7] J.-S. Hwu, S.-F. Hsu, Y.-B. Lin, and R.-J. Chen, "End-to-end security mechanisms for SMS," *Int. J. Security Netw.*, vol. 1, no. 3/4, pp. 177–183, Dec. 2006.

On Predicting Convergence of Iterative MIMO Detection-Decoding With Concatenated Codes

Andreas Ibing and Holger Boche

***Abstract*—We evaluate the applicability of methods from stochastic decoding analysis to convergence prediction of iterative multiple-input–multiple-output (MIMO) detection decoding. The one-parametric conditional Gaussian log-likelihood ratio (LLR) distribution model, which underlies EXtrinsic Information Transfer (EXIT) charts, is not adequate for some practically relevant scenarios such as fading MIMO channels. A more recent two-parametric Gaussian model, which better fits arbitrary distributions, can be combined with an offset compensation to allow for a chart-based prediction of the convergence of iterative receiver processing in these cases.**

***Index Terms*—Convergence, EXtrinsic Information Transfer (EXIT) chart, iterative detection decoding, multiple-input multiple-output (MIMO), turbo code.**

I. INTRODUCTION

Iterative detection decoding for coded multiple-input multiple-output (MIMO) transmission is known to be capable of achieving near-capacity performance [1]. The usage of iterative processing naturally leads to the question of convergence.

EXtrinsic Information Transfer (EXIT) charts are widely used for predicting and illustrating convergence of iterative decoding of concatenated codes [2], [3]. The model underlying the chart assumes that the log-likelihood ratios (LLRs) of the transmit bit values are distributed after the symbol demapper according to binary phase-shift keying (BPSK) transmission over an additive white Gaussian noise (AWGN) channel, resulting in a one-parametric conditional Gaussian distribution (conditioned on the transmit bit value).

EXIT charts have also been used to model the convergence of iterative MIMO detection decoding. In [4], they are applied to optimize irregular repeat accumulate codes for MIMO transmission and iterative receiver processing. An optimization of turbo-coded space-time block code transmission based on EXIT charts is presented in [5]. Hou *et al.* [6] used EXIT charts to analyze and optimize MIMO transmission with low-density parity-check codes.

On the other hand, in [7], it is argued that, even if the input of a log-*a posteriori* probability (APP) decoder follows a one-parametric Gaussian distribution, the output needs to be described by two parameters (mean and variance) to adequately represent the dynamics of turbo decoding. This raises questions about the applicability of the stochastic decoding analysis methods, which we elaborate on in this paper.

The contribution of this paper is to combine [2], [3], and [7], together with a new offset compensation (to account for higher order distribution moments) into a chart-based prediction method, which we verify to yield acceptable prediction accuracy for different receiver computation schedules in iterative MIMO detection decoding with turbo codes.

Manuscript received October 29, 2009; revised March 23, 2010 and May 21, 2010; accepted July 8, 2010. Date of publication August 12, 2010; date of current version October 20, 2010. The review of this paper was coordinated by Prof. N. Arumugam.

The authors are with Fraunhofer Institute for Telecommunications, Heinrich-Hertz-Institut, 10587 Berlin, Germany (e-mail: andreas.ibing@hhi.fraunhofer.de).

Color versions of one or more of the figures in this paper are available online at http://ieeexplore.ieee.org.

Digital Object Identifier 10.1109/TVT.2010.2066295

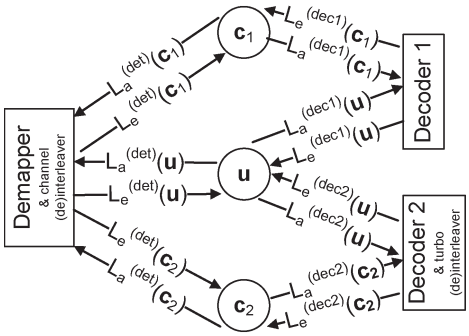

Fig. 1. Factor graph for decoding of turbo-coded MIMO transmission. The variable nodes (information bits $\mathbf{u}$ and parity bits $\mathbf{c}_1$ and $\mathbf{c}_2$) are vector valued.

II. System Model

We consider standard processing at the transmitter for turbo-coded MIMO transmission: the information bit vector $\mathbf{u}$ to transmit is transformed into code word $\mathbf{b}$ by adding code bits $\mathbf{c}_1$ of the first constituent encoder and code bits $\mathbf{c}_2$ of the second constituent encoder. For a single bit of the bit vector $\mathbf{b}$ at position i, we write b_i. At time instance t, the symbol vector $\mathbf{x}^{(t)}$ is transmitted (as part of $\mathbf{x}$) over channel matrix $\mathbf{H}^{(t)}$

$$\mathbf{y}^{(t)} = \mathbf{H}^{(t)} \cdot \mathbf{x}^{(t)}\left(\mathbf{b}^{(t)}\right) + \mathbf{n}^{(t)}. \tag{1}$$

Channel estimation is not within the scope of this paper, so that we assume perfect knowledge of channel matrices $\mathbf{H}^{(t)}$ and noise variance at the receiver. Optimum receiver performance means finding the information word with the highest APP, given the received vectors and channel knowledge

$$\hat{\mathbf{u}} = \arg\max_{\mathbf{u}} P(\mathbf{u}|\mathbf{y}, \mathbf{H}). \tag{2}$$

Since this joint detection and decoding is too complex for practical implementation, the practical approach is an iterative approximation of the information bit APPs

$$P(u_i|\mathbf{y}, \mathbf{H}) \tag{3}$$

by local computation. This is an application of the mathematical framework of Bayesian Belief Propagation [8] with loops. The conditional independencies of variables are exploited by factorizing the joint probability density function into factors that depend only on subsets of the variables. In our case, it is

$$\begin{aligned} P(\mathbf{u}, \mathbf{y}, \mathbf{H}) &= f_{\mathrm{Det}}(\mathbf{u}, \mathbf{c}_1, \mathbf{c}_2, \mathbf{y}, \mathbf{H}) f_{\mathrm{Dec1}}(\mathbf{u}, \mathbf{c}_1) \cdot f_{\mathrm{Dec2}}(\mathbf{u}, \mathbf{c}_2) \\ &= \left(\prod_t \widetilde{f_{\mathrm{Det}}}\left(\mathbf{b}^{(t)}, \mathbf{y}^{(t)}, \mathbf{H}^{(t)}\right)\right) \\ &\quad \cdot f_{\mathrm{Dec1}}(\mathbf{u}, \mathbf{c}_1) f_{\mathrm{Dec2}}(\mathbf{u}, \mathbf{c}_2). \end{aligned} \tag{4}$$

The factors are one MIMO demapper for each time instance and two constituent decoders. The corresponding receiver architecture is shown in Fig. 1 as a factor graph. (Factor graphs are described in [9] and [10].) Factor nodes perform APP computation on subsets of variables, where the involved variables are depicted as variable nodes neighboring to the factor node. A factor node outputs only the information increment gained by computation, which is often called extrinsic information [2]. To avoid the effort for normalizing probability densities and to further reduce computational effort, implementation uses LLRs, instead of bit probabilities themselves. (Multiplications are turned into additions in the log domain.) The messages passed in Fig. 1 are, therefore, vectors of LLRs. L_a denotes *a priori* LLR, and L_p denotes *a posteriori* LLR. A factor node computes *a posteriori* LLRs but outputs only the extrinsic LLRs $L_e = L_p - L_a$ [8], [9], [11]. Variable nodes compute sums of the incident LLR vectors, so that the *a posteriori* values of information bits are

$$L_p(u_i) = L_e^{(\mathrm{det})}(u_i) + L_e^{(\mathrm{dec1})}(u_i) + L_e^{(\mathrm{dec2})}(u_i). \tag{5}$$

For a decoding architecture with two factor nodes like in the case of turbo decoding without iterative demapping, the order of factor node updates is clear: the two factors are updated in turn. For our case with three nodes, the order is arbitrary (which was pointed out in the context of iterative decoding of arbitrarily concatenated codes in [3] and [12]). Based on the generic receiver architecture illustrated in Fig. 1, an actual receiver is described by its factor node update schedule.

Our aim is to predict the convergence of the described iterative receiver processing for any schedule. The approach is to track the conditional LLR distributions corresponding to the messages in Fig. 1 for all node updates. Receiver performance is then given by the mutual information (MI) between the $L_p(u)$ and the transmit bits u

$$I(u, L_p) = \sum\sum p(L_p, u) \ln \frac{p(L_p, u)}{p_{L_p}(L_p) \cdot p_u(u)} \tag{6}$$

where $p(L_p, u)$ is the joint distribution, and $p_u(u)$ and $p_{L_p}(L_p)$ are the marginal distributions.

To evaluate the accuracy of the presented prediction method for concrete demapper/decoder schemes, we pick the following common algorithms: the constituent decoders perform log-APP decoding according to the BCJR algorithm [13], and the MIMO demapper uses max-log-APP detection [1].

The extrinsic demapper LLRs are therefore [1]

$$\begin{aligned} &L_e^{(\mathrm{Det})}(b_i) \\ &\approx \max_{\mathbf{x}^{(t)} \in \mathcal{X}_i^+} \left(-\frac{1}{2\sigma_N^2} \left\| \mathbf{y}^{(t)} - \mathbf{H}^{(\mathbf{t})} \mathbf{x}^{(\mathbf{t})}\left(\mathbf{b}^{(t)}\right) \right\|^2 \right. \\ &\qquad \left. + \sum_{n \neq i} \min\left(b_n^{(t)} L_a^{(\mathrm{Det})}\left(b_n^{(t)}\right) 0\right) \right) \\ &\quad - \max_{\mathbf{x}^{(t)} \in \mathcal{X}_i^-} \left(-\frac{1}{2\sigma_N^2} \left\| \mathbf{y}^{(t)} - \mathbf{H}^{(\mathbf{t})} \mathbf{x}^{(\mathbf{t})}\left(\mathbf{b}^{(t)}\right) \right\|^2 \right. \\ &\qquad \left. + \sum_{n \neq i} \min\left(b_n^{(t)} L_a^{(\mathrm{Det})}\left(b_n^{(t)}\right) 0\right) \right) \end{aligned} \tag{7}$$

where $\mathcal{X}_i^+$ is the set of all possible transmit vectors $\mathbf{x}^{(t)}$, where the bit whose LLR is to be computed has the value $+1$. For the channel, we assume uncorrelated Rayleigh fading for each time instance t and noise variance σ_N^2. We arbitrarily pick three different schedules for which we assess prediction accuracy.

1) Schedule 1: "normal" receiver with Turbo decoder. First, the demapper is updated once; then, the constituent decoders are run alternatingly.
2) Schedule 2: the demapper is run first and then again always after four turbo decoder iterations (eight constituent decoder updates).
3) Schedule 3: "round-robin" schedule. The demapper, decoder 1, and decoder 2 are run periodically in this order (demapper update after each turbo decoder iteration).

For simulation, we further assume 4×4 quadratic phase-shift keying (QPSK) transmission and channel coding with the Third-Generation Partnership Project long-term evolution (LTE) turbo code (rate 1/3).

III. Shortcoming of One-Parametric Gaussian Model

EXIT charts [2], [3] are based on a one-parametric conditional Gaussian distribution model of LLRs. This model is derived from the assumption of BPSK transmission over an AWGN channel

$$y = x(b) + n. \tag{8}$$

Under this assumption, the extrinsic LLRs generated by the demapper follow a (conditional) Gaussian distribution with the special property that the (conditional) absolute expectancy value is half of the (conditional) variance [2]

$$\left| E\left(L_e^{(\mathrm{det})}(b) \middle| b \right) \right| = \frac{1}{2} Var\left(L_e^{(\mathrm{det})}(b) \middle| b \right). \tag{9}$$

An LLR distribution is therefore completely described by one parameter, e.g., by the standard deviation σ. As consequence, there is a bidirectional mapping $J : \sigma \mapsto I$ between this parameter and the MI carried by this distribution [the MI of LLRs with the transmit bits (6)]. This mapping is the basis of EXIT charts [2]. EXIT charts assume that the one-parametric distribution property is sustained after a BCJR decoder. The parameter transfer $I(L_a) \mapsto I(L_e)$ is tabularized in a table T, and its graph is the EXIT curve. To track LLR density evolution for convergence prediction, $I(L_e)$ can be looked up from this table for known $I(L_a)$ for information bits and code bits

$$I_e(b) = T\left(I_a(u), I_a(c)\right). \tag{10}$$

The one-parametric property (9) is also sustained for summation of LLRs since the mean and variance of the sum distribution are the sum of the means and variances, respectively. The MI of the LLR sum can therefore be determined by using J^{-1} and adding the variances [2]

$$I_{\mathrm{sum}}(u) = J\left(\sqrt{\sum_i J^{-1}\left(I_e^{(i)}(u) \right)^2} \right). \tag{11}$$

To see why this model is not adequate in our scenario, we apply EXIT charts to predict the convergence of schedule 1 ("normal" receiver with no iterative demapping) for a channel signal-to-noise ratio (SNR) of 1 dB. The prediction of MI after each factor node update is shown in Fig. 2. The figure also shows the measured MI, which we obtain by Monte Carlo simulation of the complete receiver processing and nonparametric conditional LLR distribution estimation after each factor update number. While EXIT charts predict convergence after eight node updates, measurement shows a saturation at MI of 0.53. An EXIT chart prediction for 0-dB channel SNR predicts saturation at a higher MI than 0.53. The prediction error in this case is therefore larger than 1 dB, which is so large that it renders the prediction method useless.

The misprediction is explained by the actual LLR distribution after the demapper (max-log-APP demapping [1] with uncorrelated Rayleigh fading), which is shown in Fig. 3. While it does resemble a conditional Gaussian distribution, (9) is clearly violated: the mean value is not half the variance. Fig. 3 also shows a conditional Gaussian distribution with the same MI, which satisfies (9) (mean and variance are different from the measured distribution). This is the curve that EXIT chart prediction assumes for this MI value, and it is the reason for the wrong prediction trend. The problem is not that the demapper or decoder EXIT curves would be wrong: histogram-based measurement of the extrinsic MI as in [2] is indeed correct. The problematic one-parametric fitting occurs when the output LLRs become input for the next factor node, because the EXIT curves are computed with one-parametric input distributions.

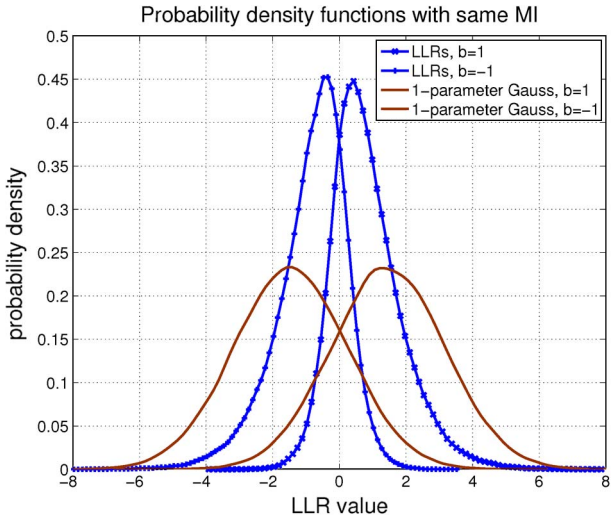

Fig. 2. For the Rayleigh-fading MIMO channel, EXIT-chart-based prediction produces a large error; in this case (4×4 QPSK, max-log-APP demapper), the prediction error corresponds to more-than-1-dB channel SNR. Simulation uses a maximum LTE packet length of 6144 information bits.

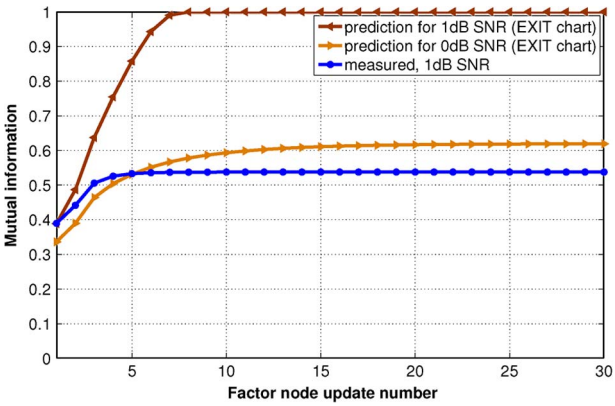

Fig. 3. LLR conditional probability density function for 4×4 QPSK MIMO transmission with uncorrelated Rayleigh fading and max-log-APP demapping. The corresponding conditional density according to the one-parametric Gaussian model is also shown: both densities have the same MI with the transmit bits.

IV. Extended Gaussian Model: Two Parameters

We note that, while EXIT charts track the MI value corresponding to an LLR distribution, they could equivalently track a different parameter describing the one-parametric Gaussian distribution, e.g., the standard deviation [7].

In the previous section, we have drawn the conclusion that the one-parametric Gaussian model where the expectancy μ is half the variance σ^2 (9) is not adequate in our scenario. However, it could still be the case that another one-parametric model, maybe with a nonlinear relation between μ and σ^2, can be used. To test this, we run a Monte Carlo simulation of the complete receiver processing according to schedule 3 ("round robin") and measure μ and σ of the LLR distributions after each factor update number. Looking at the

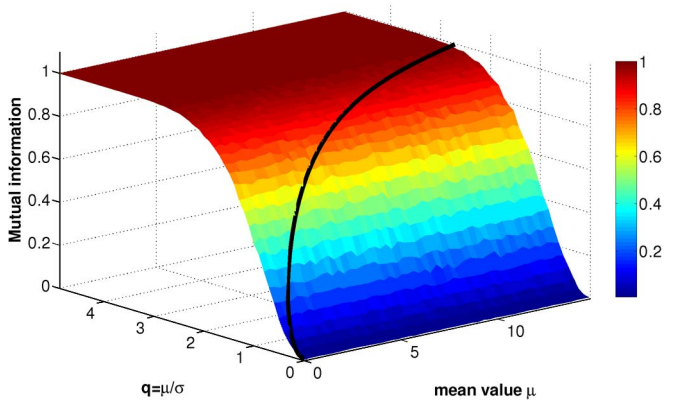

Fig. 4. Mapping LLR distribution parameters to the MI. The MI is determined by the ratio q of mean value and standard deviation. "Full" MI corresponding to a BER smaller 10^{-4} is achieved for $q > 3.7$. The one-parametric model is included as a special case and shown as a curve in the MI surface.

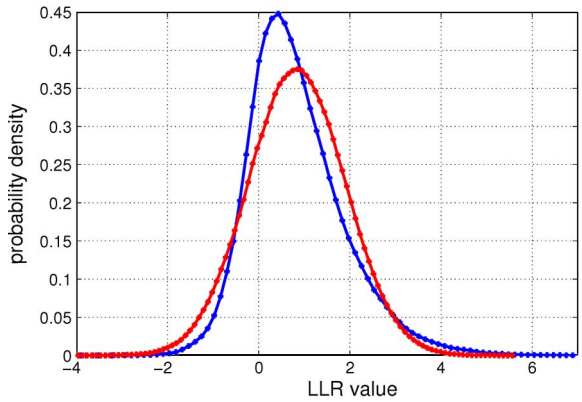

Fig. 5. LLR probability density for positive transmit bits from the example (as in Fig. 2) and the corresponding two-parametric Gaussian density. The two densities have the same mean and variance but different MIs (LLRs: 0.39; Gauss: 0.34).

value pairs of μ and σ, the result is that a one-parametric description does not work.

We therefore add one parameter to the model and, in accordance with [7], assume the LLRs as conditionally Gaussian distributed with arbitrary mean μ and standard deviation σ, leaving out (9). Table lookups for the extrinsic information transfer of decoders or demapper now have more dimensions: based on the mean and standard deviation of the input distributions, the mean and standard deviation of the extrinsic output distribution are looked up. A decoder lookup becomes

$$(\mu_e(b), \sigma_e(b)) = T\left((\mu_a(u), \sigma_a(u))\,(\mu_a(c), \sigma_a(c))\right). \tag{12}$$

The MIMO demapper lookup in our scenario has six input values (three input vectors with two parameters each, compared with Fig. 1).

The mapping from distribution parameters (μ, σ) to MI (function J) now has one dimension more. The MI of the Gaussian distribution is only determined by the ratio $q = \mu/\sigma$ of mean value and standard deviation, and the corresponding bit error rate (for *a posteriori* LLRs) is given by the tail probability [7]

$$\text{BER} = Q(q). \tag{13}$$

As coordinates for the 2-D mapping function, we therefore use mean value μ, quotient $q = \mu/\sigma$, and MI

$$J : \left(\mu, \frac{\mu}{\sigma}\right) \mapsto I. \tag{14}$$

The function is shown in Fig. 4. The figure also shows the curve for the one-parametric case, which is embedded as a special case in the MI surface.

A bit error rate (BER) smaller than 10^{-4} corresponds to $q > 3.7$. Fig. 4 therefore also shows the parameter range, which has to be covered by the lookup tables. Since there are infinitely many Gaussian distributions with the same q, the function J is no longer invertible. Due to this, the distributions are tracked for iterative decoding using only their Gaussian parameters μ and σ, and the mapping to MI (or BER) is only necessary when the iterations are stopped. For a sum of LLRs, we now have, instead of (11)

$$\begin{aligned} \mu^{(\text{sum})}(u) &= \sum_i \mu^{(i)}(u) \\ \sigma^{(\text{sum})}(u) &= \sqrt{\sum_i \left(\sigma^{(i)}\right)^2} \end{aligned} \tag{15}$$

i.e., the sum is still (conditionally) Gaussian distributed.

V. Compensating the MI Offset for Higher Order Moments of LLR Distribution

As expected, the more flexible two-parametric model reproduces the actual MI evolution trend and yields better accuracy, but beginning from the first demapping, the prediction has an MI offset, compared with the measured MI. This offset can be explained by the fact that the MIMO demapper LLRs do not exactly follow a Gaussian distribution: not all cumulants of the distribution for an order larger than 2 are zero. This is shown in Fig. 5. The figure shows the LLR distribution from the MIMO example and the Gaussian distribution, which has the same mean and variance. The measured LLR distribution shows a nonzero skewness; it is not symmetric. The MI of the assumed Gaussian distribution is smaller, causing the initial prediction offset. The Gaussian distribution we assume can have either the same mean and variance as the real distribution or the same MI but not both.

For a consistent concatenation of table lookups, we determine the demapper table using the Gaussian distribution with the same mean and variance as the real one. To compensate the initial MI loss, we also compute it at table generation time. For one channel SNR value, the demapper table now is a mapping from six input dimensions to three output dimensions (compared with Fig. 1)

$$\begin{aligned} &(\mu_e(b), \sigma_e(b), I_{\text{offset}}) \\ &\quad = T\left((\mu_a(u), \sigma_a(u))\,(\mu_a(c_1), \sigma_a(c_1))\,(\mu_a(c_2), \sigma_a(c_2))\right). \end{aligned} \tag{16}$$

Adding the channel SNR as input dimension makes the demapper table input 7-D. For the prediction results in this paper, we sampled the input LLR distributions with eight points per dimension ($0 \le \mu \le 15,\ 0 \le q \le 5$), resulting in 260 000 entries in the demapper table per channel SNR value. Using the fact that the roles of u, c_1, and c_2 are interchangeable for the demapper, only 46 000 table entries have to be computed. The table for a constituent decoder was already described in the previous section (four input dimensions to two output dimensions). Since the two constituent decoders are identical for the LTE turbo code we used, they are both described by the same table. For table lookups, we use linear interpolation between neighboring sample points.

The predicted Gaussian parameters (μ_p, σ_p) of the distribution of the *a posteriori* LLRs $L_p(u)$ are then mapped to MI by table lookup (function J), and the I_{offset} value returned by the last demapper table lookup for $L_e^{(\text{det})}(b)$ is added, i.e.,

$$I_{\text{predict}} = J\left(\mu_p, \frac{\mu_p}{\sigma_p}\right) + I_{\text{offset}}. \tag{17}$$

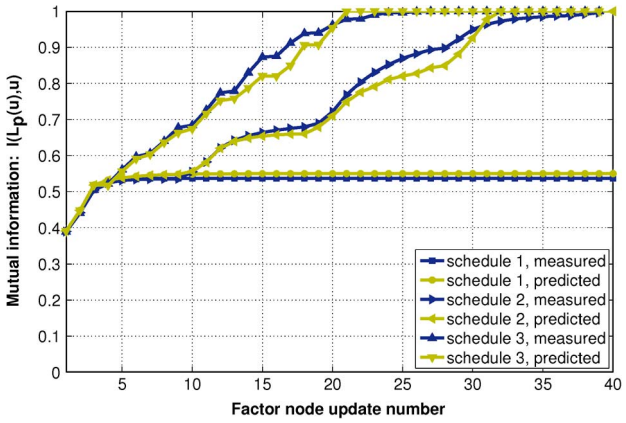

Fig. 6. Verifying MI prediction accuracy: predicted and measured MIs for the three different schedules (with a packet length of 6144 information bits).

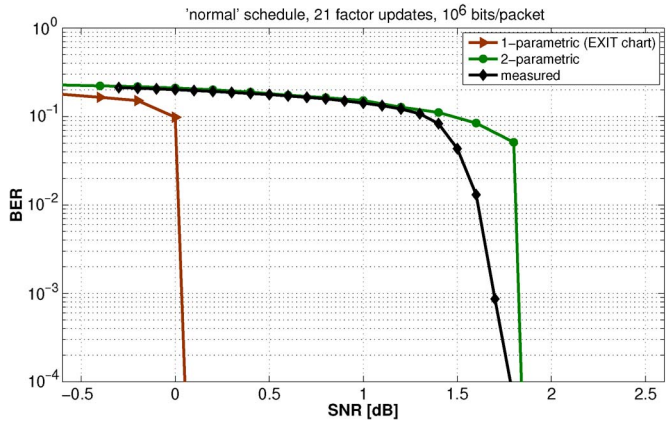

Fig. 7. Predicted and measured BERs for one example schedule, using very long packets (10^6 bits). The curves for a smaller packet length (6144 information bits) differ only insignificantly.

VI. MI Prediction Accuracy for Different Schedules

We verify MI prediction accuracy by comparison with MI measurement, for the three receiver processing schedules described in Section II. "Prediction" uses the described concatenation of table lookups, where the concatenation order of lookups from the two tables is determined by the schedule. "Measurement" performs Monte Carlo simulation of the complete receiver and measures MI using nonparametric estimation of the joint distribution of *a posteriori* LLRs and transmit bits according to (6), independently for each schedule.

The results of prediction and measurement are shown in Fig. 6. Schedule 1 ("normal" receiver) does not converge for this low SNR level, which is now correctly predicted. The MI of *a posteriori* LLRs saturates after around seven factor computations (six constituent decoder updates) at 0.53. Schedule 2 converges after around 40 factor computations (including five demapper updates and 35 constituent decoder updates). A demapper update only brings a small MI improvement in itself, but, afterward, decoder updates gain more again. Schedule 3 ("round-robin") converges already with around 25 factor computations.

All periodic schedules, which include the same factors, converge to the same MI limit value [3] since they completely use the same information sources. The maximum MI value, which can be reached by the extrinsic MIMO demapper output $L_e^{(\mathrm{det})}$, is that of single-input–multiple-output maximum ratio combining for (shifted) BPSK modulation [14]: if the demapper *a priori* LLRs $L_a^{(\mathrm{det})}$ have full MI (implying that the receiver algorithm has already converged) for each LLR to compute, all transmit bits of the MIMO vector are known, except one, meaning that only two symbol constellation points remain.

The MI prediction curves in Fig. 6 do show small deviations from the also shown measurement curves, which are due to higher order cumulants (order higher than 2) of LLR distributions and the finite granularity of the lookup tables.

VII. Verifying BER and Threshold Prediction

Prediction of the APP LLR distribution includes BER prediction according to (13). To verify BER and SNR threshold prediction, we apply this mapping from the LLR distribution to BER for the two models and compare with measurement for very long packets. For the proposed method, we have

$$\mathrm{BER} = Q\left(\frac{\mu_p}{\sigma_p}\right) \tag{18}$$

whereas, for EXIT-chart-based prediction, this reduces to one parameter

$$\mathrm{BER} = Q\left(\sqrt{\frac{\mu_p}{2}}\right). \tag{19}$$

We evaluate prediction and measurement for varying SNRs (for a fixed schedule), with focus on the SNR threshold required for a target BER, e.g., 10^{-4}. Fig. 7 illustrates results for the "normal" schedule with 21 factor updates. As implied by MI prediction (Fig. 3), EXIT charts predict the threshold for this schedule to be more than 1.5 dB too small, whereas the proposed method predicts it to be 0.1 dB too high. For BER prediction, no compensation is applied to the MI offset, as this would affect the complete BER curve and not only the BER threshold. The MI offset causes the SNR threshold to be predicted too high.

VIII. Discussion

EXIT charts in the normal way as applied to AWGN channels are not applicable to some practically relevant scenarios with fading MIMO channels. How well the underlying one-parametric model fits the demapper LLR distribution depends on the demapper algorithm, modulation, and MIMO fading distribution. This may explain why our results seem to differ from [6], where a "good match" was found between simulation and EXIT-chart-based prediction in a different scenario.

The two-parameter extension improves prediction performance by better fitting to the real LLR distribution. Together with offset compensation for higher order distribution moments, it achieves satisfactory MI prediction accuracy. For non-Gaussian distributions, a systematic error remains (higher order moments), so that prediction performance is less accurate than for AWGN channels. Prediction accuracy for other channel models—particularly intersymbol interference (ISI) channels—has not been investigated. The proposed method is however applicable to MIMO orthogonal frequency-division multiplexing (OFDM), as OFDM converts an ISI channel into a set of individually flat-fading channels.

The higher dimensionality of the extended charts causes the charts to be less illustrative. Complexity of lookup table computation increases due to the higher dimensionality. On the other hand, computational effort is reduced again a bit by the parametric density estimation: estimating mean and variance is faster than estimating MI (with

nonparametric density estimation like histograms or kernel methods). This could also be used for computation of normal EXIT charts, as it is also consistent with the one-parametric model. In principle, the prediction accuracy can be improved by increasing the number of parameters used to describe LLR distributions: lookup tables could be extended to include higher order moments. This is limited in practice by the time needed to compute the tables, and the advantage of fast prediction, compared to slow link-level simulation, would erode.

The proposed prediction method may serve as a basis for receiver optimization at receiver design time (choice of algorithms and processing schedule). Comparing all receivers for the described scenario (three factor nodes), which have a schedule length of exactly 20 factor node updates (10^6 different receivers), may well be too much for link-level simulation-based comparison. Using the proposed method, all of them can be compared after generating only two lookup tables. Comparison of different factor computation algorithms (particularly demapper algorithm alternatives) can be done by changing the respective factor lookup table. A criterion for optimization can be the sum computational cost for reaching the target MI (corresponding to a required packet error rate) at a certain SNR. The prediction accuracy of the proposed method is sufficient to reduce the receiver design space to a few interesting algorithm candidates, which can then be verified by more time-consuming link-level simulation.

REFERENCES

[1] B. Hochwald and S. ten Brink, "Achieving near-capacity on a multiple-antenna channel," *IEEE Trans. Commun.*, vol. 51, no. 3, pp. 389–399, Mar. 2003.

[2] S. ten Brink, "Convergence behavior of iteratively decoded parallel concatenated codes," *IEEE Trans. Commun.*, vol. 49, no. 10, pp. 1727–1737, Oct. 2001.

[3] F. Brännström, L. Rasmussen, and A. Grant, "Convergence analysis and optimal scheduling for multiple concatenated codes," *IEEE Trans. Inf. Theory*, vol. 51, no. 9, pp. 3354–3364, Sep. 2005.

[4] G. Yue and X. Wang, "Optimization of irregular repeat-accumulate codes for MIMO systems with iterative receivers," *IEEE Trans. Wireless Commun.*, vol. 4, no. 6, pp. 2843–2855, Nov. 2005.

[5] Y. Ueng, C. Yeh, M. Lin, and C. Wang, "Turbo coded multiple-antenna systems for near-capacity performance," *IEEE J. Sel. Areas Commun.*, vol. 27, no. 6, pp. 954–964, Aug. 2009.

[6] J. Hou, P. Siegel, and L. Milstein, "Design of multi-input, multioutput systems based on low-density parity-check codes," *IEEE Trans. Commun.*, vol. 53, no. 4, pp. 601–611, Apr. 2005.

[7] M. Fu, "Stochastic analysis of turbo decoding," *IEEE Trans. Inf. Theory*, vol. 51, no. 1, pp. 81–100, Jan. 2005.

[8] J. Pearl, *Probabilistic Reasoning in Intelligent Systems: Networks of Plausible Inference*, 2nd ed. San Mateo, CA: Morgan Kaufmann, 1988.

[9] F. Kschischang, B. Frey, and H. Loeliger, "Factor graphs and the sum-product algorithm," *IEEE Trans. Inf. Theory*, vol. 47, no. 2, pp. 498–519, Feb. 2001.

[10] C. Bishop, *Pattern Recognition and Machine Learning*. New York: Springer-Verlag, 2006.

[11] R. McEliece, D. MacKay, and J. Cheng, "Turbo decoding as an instance of Pearl's 'belief propagation' algorithm," *IEEE J. Sel. Areas Commun.*, vol. 16, no. 2, pp. 140–152, Feb. 1998.

[12] S. Benedetto, G. Montorsi, D. Divsalar, and F. Pollara, "Soft-input soft-output modules for the construction and distributed iterative decoding of code networks," *Eur. Trans. Telecommun.*, vol. 9, no. 2, pp. 155–172, Mar./Apr. 1998.

[13] L. Bahl, J. Cocke, F. Jelinek, and J. Raviv, "Optimal decoding of linear codes for minimizing symbol error rate," *IEEE Trans. Inf. Theory*, vol. IT-20, no. 2, pp. 284–287, Mar. 1974.

[14] A. Ibing, D. Kühling, and H. Boche, "On the relation of MIMO APP detection and SIMO maximum ratio combining," in *Proc. IEEE GLOBECOM*, 2009, pp. 1444–1449.

Superresolution TOA Estimation With Computational Load Reduction

Nam-Ryul Jeon, Han-Byul Lee, Chan Gook Park, Seong Yun Cho, and Seong-Cheol Kim, *Member, IEEE*

***Abstract*—Although the superresolution multipath delay profile (MDP) estimation technique enhances the time resolution of a low-resolution MDP by using matrix computations, the computational load for the matrix computations is a problem, because it drastically increases with the length of the MDP. Because positioning systems require the time of arrival (TOA) of the first path only, it is possible to reduce the computational load by applying the matrix computations only to the part of the MDP that is narrowed but still includes the TOA of the first path. This paper proposes a scheme for determining the observation window of MDP from the low-resolution TOA estimates, which are obtained from the MDPs produced by the pseudonoise correlation method. The proposed scheme makes use of the random nature of the low-resolution TOA estimates to further reduce the observation window. The computational efficiency and estimation accuracy of the proposed scheme are examined by channel simulations based on the Saleh–Valenzuela indoor channel model and are also compared with the computational efficiency and estimation accuracy of the conventional superresolution technique without the observation window reduction.**

***Index Terms*—Computational efficiency, indoor positioning, superresolution time-of-arrival (TOA) estimation.**

NOMENCLATURE

Bold symbols	Matrices or vectors.
$(\cdot)^{\mathrm{T}}$	Matrix transpose operation.
$(\cdot)^{\mathrm{H}}$	Hermitian transpose operation.
$\delta(\cdot)$	Dirac delta function.
$\lceil \mathrm{x} \rceil$	Smallest integer larger than or equal to x.
$\lfloor \mathrm{x} \rfloor$	Largest integer smaller than or equal to x.
$\mathrm{E}[\cdot]$	Expectation.
$\min(\cdot)$	Minimum.
$\max(\cdot)$	Maximum.

I. INTRODUCTION

Determining the distance from the time of arrival (TOA) is the most popular ranging method for accurate positioning systems. To find the TOA, the pseudonoise (PN) sequence has been used in positioning

Manuscript received January 11, 2009; revised October 27, 2009, March 24, 2010, and May 17, 2010; accepted June 25, 2010. Date of publication August 3, 2010; date of current version October 20, 2010. This work was supported in part by the Korean Government through the Korea Science and Engineering Foundation under Grant 2009-0080852 and in part by the IT R&D program (2007-F-040-01, Development of Indoor/Outdoor Seamless Positioning Technology) of the Institute for Information Technology Advancement, Ministry of Information and Communication. The review of this paper was coordinated by Prof. X. Wang.

N.-R. Jeon, H.-B. Lee, and S.-C. Kim are with the Department of Electrical Engineering, Institute of New Media and Communications, Seoul National University, Seoul 151-742, Korea (e-mail: jeon3115@maxwell.snu.ac.kr; hblee@maxwell.snu.ac.kr; sckim@maxwell.snu.ac.kr).

C. G. Park is with the School of Mechanical and Aerospace Engineering, Institute of Advanced Aerospace Technology, Seoul National University, Seoul 151-744, Korea (e-mail: chanpark@snu.ac.kr).

S. Y. Cho is with the Vehicle IT Convergence Research Department, Electronics and Telecommunications Research Institute, Daejeon 305-700, Korea (e-mail: sycho@etri.re.kr).

Digital Object Identifier 10.1109/TVT.2010.2063044